

Revision 1

Jingwenite-(Y) from the Yushui Cu deposit, South China: the first occurrence of a V-HREE-bearing silicate mineral

Peng Liu^{1*}, Xiangping Gu^{2*}, Wenlan Zhang³, Huan Hu³, Xiaodan Chen⁴, Xiaolin Wang³,
Wenlei Song¹, Miao Yu², Nigel J. Cook⁵

¹ *State Key Laboratory of Continental Dynamics, Department of Geology, Northwest University, Xi'an 710069, China*

² *School of Geosciences and Info-Physics, Central South University, Changsha, Hunan 410083, China*

³ *State Key Laboratory for Mineral Deposits Research, School of Earth Sciences and Engineering, Nanjing University, Nanjing 210023, China*

⁴ *MLR Key Laboratory of Metallogeny and Mineral Assessment, Institute of Mineral Resources, Chinese Academy of Geological Sciences, Beijing 100037, China*

⁵ *School of Civil, Environmental and Mining Engineering, The University of Adelaide, Adelaide, SA 5005, Australia*

Corresponding author: Peng Liu, penqliu@nwu.edu.cn

Xiangping Gu, guxp@csu.edu.cn

ABSTRACT

21
22 Jingwenite-(Y), $Y_2Al_2V^{4+}_2(SiO_4)O_4(OH)_4$, the first V-HREE-bearing silicate
23 mineral discovered in nature, is an abundant component of a sediment-hosted stratiform Cu
24 (SSC) deposit, Yushui, in South China. The mineral occurs in bedded/massive sulfide-
25 bearing ore and is associated with bornite, chalcopyrite, galena, xenotime-(Y), nolanite,
26 thortveitite, roscoelite, barite, and quartz. Optically, jingwenite-(Y) is biaxial (+), with $\alpha =$
27 $1.92(4)$, $\beta = 1.95(2)$, $\gamma = 1.99(3)$ (white light), and $2V$ (calculated) = 83° . The dispersion is
28 medium with $r < v$, and the pleochroism is with X = light brown, Y = brown, Z = dark brown.
29 The colour, streak, lustre, and hardness (Mohs) are light brown, yellowish grey, vitreous, and
30 $4\frac{1}{2}$ –5, respectively.

31 Jingwenite-(Y) is monoclinic, with space group $I2/a$, $Z = 4$, and unit-cell parameters $a =$
32 $9.4821(2)$ Å, $b = 5.8781(1)$ Å, $c = 19.3987(4)$ Å, $\beta = 90.165(2)^\circ$, and $V = 1081.21(4)$ Å³. The
33 structure of jingwenite-(Y) has chains of edge-sharing Al (V, Fe)-O octahedra and V (Ti)-O
34 octahedra extending along the b -axis and linked by insular Si-O tetrahedra, leaving open
35 channels occupied by HREEs. Jingwenite-(Y) is a new nesosilicate structural type.

36 Sm-Nd dating and Nd isotope signatures of jingwenite-(Y) reveal an epigenetic origin
37 and suggest that HREEs and V were added to the SSC system via leaching of abundant
38 heavy minerals in the footwall red sandstone by oxidized basinal brines. The abundance of
39 jingwenite-(Y) at Yushui indicates that it could potentially be a valuable resource for HREE
40 and V. Moreover, HREE and V mineralization can also occur in the same sediment-hosted
41 Cu mineral system.

42 **Keywords:** New mineral; Jingwenite-(Y); Heavy Rare Earth Elements; Yushui;

INTRODUCTION

43
44 Both heavy rare earth elements (HREE: Gd–Lu + Y) and vanadium (V) are critical and highly
45 valuable metals increasingly needed for high–technology applications, e.g., in the aerospace
46 industry and in the transition to low–carbon energy generation ([Hatch, 2012](#)). Here we report
47 a new mineral, jingwenite–(Y), ideally $Y_2Al_2V^{4+}_2(SiO_4)_2O_4(OH)_4$, the first V–HREE–bearing
48 silicate mineral discovered in nature. It occurs as an abundant phase in a sediment–hosted
49 stratiform Cu deposit (SSC) ([Liu et al., 2022](#)), the Yushui deposit, South China, which could
50 potentially be a valuable resource of HREE and V. Jingwenite–(Y) has been approved by the
51 International Mineralogical Association Commission on New Minerals, Nomenclature and
52 Classification (IMA2021–070). The new mineral jingwenite–(Y) is named in honor of
53 Professor Jingwen Mao (born in 1956). He is a leading Chinese economic geologist at the
54 China University of Geosciences (Beijing), with global impact from his publication output and
55 significant contribution to international professional associations. Type material is deposited
56 in the mineralogical collections of the Geological Museum of China, catalog number
57 M16122.

OCCURRENCE AND ASSOCIATED MINERALS

58
59 Jingwenite–(Y) is found in Cu–sulfide ore from the Yushui deposit, an SSC ore system
60 located about 16 km northeast of Meizhou City, Guangdong Province, China (24°25'18"N,
61 116°11'48"E) ([Fig. 1A](#)). The Yushui deposit is concealed beneath Late–Jurassic volcanic
62 cover and is hosted mainly within sedimentary rocks at the unconformity between Upper
63 Carboniferous dark–grey dolostone and a >300 m–thick sequence of Lower Carboniferous
64 red sandstone ([Fig. 1B](#)) characterized by an abundance of heavy minerals including

65 xenotime-(Y), rutile, zircon, and hematite. There are three ore types: I) bedded/massive; II)
66 disseminated; and III) vein-type. Jingwenite-(Y) occurs mainly in bedded/massive ore
67 (orebody V₁), where associated minerals are bornite, chalcopyrite, galena, xenotime-(Y),
68 nolanite, thortveitite, roscoelite, barite, quartz, and an as-yet unnamed V-HREE-Sc-
69 bearing silicate mineral phase (Fig. 2).

70 ANALYTICAL METHODS

71 Polished sections were prepared from the jingwenite-(Y) specimen for major element and
72 Sm-Nd isotope analysis.

73 Chemical composition analysis

74 Quantitative major-element analysis of minerals was done at the State Key Laboratory of
75 Mineral Deposits Research, School of Earth Sciences and Engineering, Nanjing University,
76 using a JEOL JXA-8530F electron microprobe. All measurements were done using an
77 accelerating voltage of 15 kV, a beam current of 50 nA, and a beam size of 2 μm. The
78 analyzing crystals were PETJ (V and Y), LIFH (Fe, Nd, Sm, Gd, Tb and Ti), LIFL (Dy, Ho, Er,
79 Tm, Yb and Lu), LDE1L (F) and TAP (Si and Al). The K α line was chosen for analysis of Si,
80 Al, Fe, V and Ti; the L α line for Sm, Nd, Tb, Gd, Dy, Er, Tm, Yb and Y; and the L β line for Ho
81 and Lu. The counting times on peaks were 10 s for Si, Al and F; 20 s for Fe, V, Ti, Sm, Gd,
82 Dy, Er, Ho, and Y; and 30 s for Nd, Tb, Tm, Yb, and Lu. Background intensities were
83 measured on both sides of the peak for half of the peak time. The standards were REE1 for
84 Gd, Tb, and Tm, REE2 for Nd, Sm, Yb, and Lu, and REE4 for Dy, Ho, and Er; albite for Si;
85 amphibole (B5) for Al, Fe, Ca, and Ti; synthetic YPO₄ for Y; Ca₃(VO₄)₂ for V.

86 **Crystal–structure analysis**

87 X–ray powder and single–crystal diffraction was done at the School of Geosciences and
88 Info–Physics, Central South University, China, with a Rigaku XtaLAB Synergy diffractometer
89 (CuK α radiation) in powder Gandolfi mode at 50 kV and 1 mA, and a Rigaku XtaLAB
90 Synergy diffractometer equipped with CuK α radiation at 50 kV and 1 mA.

91 **Raman spectroscopy analysis**

92 Raman spectroscopy of jingwenite–(Y) was done on a Horiba LabRAMIS spectrometer
93 using the 532 nm line of laser at the State Key Laboratory for Mineral Deposits Research,
94 Nanjing University. The laser beam (532 nm, laser power 20 mW) was focused to 1 μm with
95 a 100 \times objective in an Olympus microscope. The time of each scan in the range 100–4000
96 cm^{-1} was 20–60 s (3 accumulated times) with a resolution of 2 cm^{-1} .

97 **LA–MC–ICP–MS Sm–Nd isotope analysis**

98 Neodymium isotopic ratios of jingwenite–(Y) were measured by LA–MC–ICP–MS at Nanjing
99 FocuMS Technology Co. Ltd, Jiangsu province, China, with an Australian Scientific
100 Instruments *RESOLution LR* laser–ablation system (Canberra, Australia) and Nu Instruments
101 *Nu Plasma II* MC–ICP–MS (Wrexham, Wales, UK). The 193 nm ArF excimer laser,
102 homogenized by a set of beam delivery systems, was focused on the surface with fluence of
103 4.5 J/cm^2 . Helium (370ml/min) was used as carrier gas to transport aerosol out of the
104 ablation cell, and was mixed with argon (~ 0.97 L/min) via T–connector before entering ICP
105 torch. Integration time of *Nu Plasma II* was set to 0.3 s (equating to 133 cycles during the 40
106 s). For Sm–Nd isotope analyses, each acquisition incorporated 20 s background (gas blank),
107 followed by ablation with spot diameters of 40 μm , and 75 μm , respectively, at 5 Hz repetition

108 rate for 40 s.

109 The isobaric interference of ^{144}Sm on ^{144}Nd is significant. The $^{147}\text{Sm}/^{149}\text{Sm}$ ratio (1.0868)
110 and the measured $^{147}\text{Sm}/^{149}\text{Sm}$ ratio were used to calculate the Sm fractionation factor, and
111 then used the measured ^{147}Sm intensity and the natural $^{147}\text{Sm}/^{144}\text{Sm}$ ratio were used to
112 correct the Sm interference on mass 144. The interference-corrected $^{146}\text{Nd}/^{144}\text{Nd}$ ratio was
113 then normalized to 0.7219 to calculate the Nd fractionation factor. Then the $^{143}\text{Nd}/^{144}\text{Nd}$ and
114 $^{145}\text{Nd}/^{144}\text{Nd}$ ratios were normalized using the exponential law. Standard monazites (44069,
115 M2, M4, Trebilcock, and Namaqualand-2) and apatites (MAD, Durango, OtterLake, AP1,
116 and AP2) were treated as quality control every ten unknown samples. The $^{147}\text{Sm}/^{144}\text{Nd}$ ratio
117 was calculated using the exponential law after correcting for the isobaric interference of
118 ^{144}Sm on ^{144}Nd as described above, and then was externally calibrated against the
119 $^{147}\text{Sm}/^{144}\text{Nd}$ ratio of the standard monazite (Namaqualand-2: $^{147}\text{Sm}/^{144}\text{Nd}=0.0980\pm 3$, ID-
120 TIMS by [Liu et al. 2012](#)).

121 RESULTS

122 Optical, morphological, and physical properties of Jingwenite-(Y)

123 Jingwenite-(Y) occurs as brown aggregates up to 280 μm in size consisting of platy and
124 columnar crystals, individually ranging from 5 to 30 μm . The method of the measurement of
125 refractive index allows the Fresnel equations to be directly used to calculate the refractive
126 index with the measured diffuse reflectance. More details are provided in Tolosa et al. (2011).
127 Optically, jingwenite-(Y) is biaxial (+), with $\alpha = 1.92(4)$, $\beta = 1.95(2)$, $\gamma = 1.99(3)$ (white light),
128 and $2V$ (calculated) = 83° . The dispersion is medium with $r < v$, and the pleochroism is with X
129 = light brown, Y = brown, Z = dark brown. The $a:b:c$ ratio from single-crystal X-ray

130 diffraction data is 0.489:0.303:1. The colour, streak, lustre, and hardness (Mohs) are light
131 brown, yellowish grey, vitreous, and 4½–5, respectively. The calculated density is 4.475
132 g/cm⁻³ based on the empirical formula and unit cell volume determined from single crystal
133 XRD data.

134 **Chemical composition**

135 Jingwenite–(Y) displays narrow ranges of SiO₂ and Al₂O₃ contents of 16.07–16.67 wt% and
136 10.10–11.66 wt%, respectively, and variable contents of VO₂, TiO₂, Y₂O₃, Dy₂O₃, Er₂O₃,
137 Yb₂O₃, and Lu₂O₃ ranging from 25.06 to 28.31 wt%, 0.06 to 3.74 wt%, 21.97 to 27.43 wt%,
138 2.54 to 4.23 wt%, 2.80 to 4.37 wt%, 2.86 to 5.86 wt%, and 1.21–4.01 wt%, respectively, with
139 low Fe₂O₃, Gd₂O₃, Tb₂O₃, Ho₂O₃, and Tm₂O₃ contents of ~1.87 wt%, 0.45–0.94 wt%, 0.22–
140 0.52 wt%, 0.63–1.04 wt%, and 0.39–0.87 wt% ([Table S1](#)).

141 The empirical formula, calculated on the basis of 16 apfu O, is
142 (Y_{1.54}Yb_{0.14}Er_{0.14}Dy_{0.12}Lu_{0.08}Ho_{0.04}Gd_{0.02}Tm_{0.02}Tb_{0.02})_{Σ2.12}(Al_{1.5}V_{0.38}Fe_{0.08})_{Σ1.96}(V_{1.84}Ti_{0.16})_{Σ2}(Si
143 O₄)_{1.94}O_{4.6}(OH)_{3.64}, which can be simplified to
144 (Y,Yb,Er,Dy)₂(Al,V³⁺,Fe³⁺)₂(V⁴⁺,Ti)₂(SiO₄)₂O₄(OH)₄. The type and amount of OH were
145 determined from bond–valence calculations of O atoms in the crystal structure, and the
146 Raman spectrum of jingwenite–(Y) ([Fig. S1](#)).

147 **Crystal structure**

148 Unit–cell parameters obtained from the single–crystal and powder X–ray diffraction data ([Fig.](#)
149 [S2](#); [Tables S2](#), [S3](#)) are: $a = 9.4821(2)$ Å, $b = 5.8781(1)$ Å, $c = 19.3987(4)$ Å, $\beta = 90.165(2)^\circ$,
150 and $V = 1081.21(4)$ Å³, and $a = 9.5166(6)$ Å, $b = 5.8967(3)$ Å, $c = 19.4557(8)$ Å, $\beta =$
151 $90.111(4)^\circ$, and $V = 1090.63(7)$ Å³, respectively. The crystal structure of jingwenite–(Y) was

152 determined and refined using SHELX (Sheldrick, 2015a, b); crystallographic data and
153 refinement statistics are given in Table S3. The structure was solved in space group *I2/a* and
154 refined with anisotropic vibrations for all sites. The occupancies of atoms are refined toward
155 minimum *R*1 and show good agreement with chemical composition. For simplicity, only Y, Dy,
156 Er and Yb are considered in the refinement for rare earth elements (REE) as they are the
157 dominant elements according to microprobe analyses. The final anisotropic full-matrix
158 least-squares refinement on F^2 for 111 parameters converged at *R*1 = 2.46%, *wR*2 = 6.92%
159 for 874 independent reflections ($I > 4\sigma(I)$) and *R*1 = 2.67%, *wR*2 = 6.99% for all 5274
160 reflections. The final atomic coordinates and displacement parameters are listed in Table 1,
161 and selected bond lengths and angles are presented in Table 2. The bond-valence sums of
162 atoms were calculated using parameters given by Brese and O'Keeffe (1991) (Table 3; Fig.
163 3).

164 **Raman spectrum**

165 The Raman spectrum of jingwenite-(Y) shows the bands of O–H stretching vibrations at
166 2937, 3176, 3486 and 3568 cm^{-1} , the bands of Si–O stretching vibrations at 824, 847, 897
167 and 1008 cm^{-1} , the bands of Al–O, V–O, Y–O vibrations in the range of 100–700 cm^{-1} (Fig.
168 S1).

169 **In-situ Sm–Nd isotope composition**

170 Twenty *in-situ* spot analyses of jingwenite-(Y) gave a Sm–Nd isochron age of 217 ± 25 Ma
171 (2σ , MSWD=4.0) (Fig. 4A), which is comparable, within uncertainty, to the HREE and U
172 mineralization age of ca. 223 Ma using U–Pb and Sm–Nd dating of uraninite, xenotime-(Y)
173 and hingganite-(Y) (Liu et al., 2022). The $\epsilon_{\text{Nd}(t)}$ values were calculated using an age of 223

174 Ma for HREE mineralization and range from -13.0 to -9.7 (Fig. 4B; Table S4).

175 DISCUSSION

176 The structure of jingwenite-(Y) is composed of *b*-axis-oriented chains of octahedra
177 consisting of edge-sharing Al (V, Fe)-O octahedra and V (Ti)-O octahedra linked by insular
178 Si-O tetrahedra, leaving open channels occupied by rare earth elements (Fig. 3). In the
179 chains of Al-O octahedra chain, two alternative cation sites, Al1 and Al2, share edges O4-
180 O4 and O7-O7. Both sites are dominated by Al but with incorporation of Fe³⁺, V³⁺, more in
181 Al2 than in Al1. In the chains of V-O octahedra, the V-O octahedra share the edge O5-O6
182 and are strongly distorted with respect to the major difference between the shortest V-O6
183 distance (1.664 Å) and the longest V-O6 distance (2.406 Å). The Si-O tetrahedra share O2,
184 O4 with two separate chains of Al-O octahedra and share O1, O3 with two neighboring V-O
185 octahedra in the same chains of V-O octahedra. Rare earth elements are 8-coordinated
186 and occupy open channels along the *b*-axis with the REE-O distances ranging from 2.302 Å
187 to 2.409 Å (average 2.353 Å). Bond valence calculations show that V1 site is dominated by
188 V⁴⁺ and hydrogen atoms are attached with two oxygen atoms (O7, O8), leading to the ideal
189 crystal chemical formula $Y_2Al_2V^{4+}_2(SiO_4)_2O_4(OH)_4$. The edge-sharing chains of V⁴⁺-O
190 octahedra also occur in synthetic VO₂ (C2/m) (Marezio et al. 1972) and VO₂ (P2₁/c) (Longo
191 and Kierkegaard, 1970), in which V-O bond lengths vary from 1.73 Å to 2.13 Å. The crystal
192 structure of jingwenite-(Y) may represent a new structural type of nesosilicate and could
193 therefore be classified as a new group with a Dana classification number 52.4.10.1, or a new
194 series with a Strunz classification number 8/B.39.1.

IMPLICATIONS

195
196 The Sm–Nd isochron age of 217 ± 25 Ma for jingwenite–(Y) indicates an epigenetic origin.
197 Furthermore, our recent studies (Liu et al., 2022) showed that the HREEs and U were
198 leached from the footwall sandstone, which contains abundant heavy minerals, by oxidized
199 basinal brines, and mobilized into the SSC system. The similar $\epsilon_{\text{Nd}(t)}$ values (-13.0 to -9.7) of
200 jingwenite–(Y) also support an identical sedimentary source. Vanadium can be dissolved
201 and transported in oxidized fluids as V^{5+} , whereas V^{4+} and V^{3+} are insoluble in hydrothermal
202 fluids and preferentially partition into mineral phases (Fischer, 1973; Huang et al., 2015a). In
203 jingwenite–(Y), V occurs mainly as V^{4+} while the crystal structure indicates that V^{3+} can
204 substitute for Al^{3+} in $\text{Y}_2\text{Al}_2\text{V}^{4+}_2(\text{SiO}_4)_2\text{O}_4(\text{OH})_4$. Thus, just like HREE and U, V is also likely
205 leached and transported as V^{5+} by oxidized fluids, then reduced to insoluble V^{4+} or V^{3+} by
206 organic-rich beds in the overlying dolostone/limestone, where it is precipitated and forms
207 into jingwenite–(Y).

208 Collectively, the abundance of jingwenite–(Y) at Yushui not only indicates that it could
209 potentially be a valuable resource for HREE and V but also highlights that HREE and V
210 mineralization can also occur in the same sediment-hosted Cu mineral system.

ACKNOWLEDGMENTS

211
212 We thank Guoguang Wang, Xiaochun Li, Changhui Ke, Wei Jian, and Liang Li for their
213 insightful discussion and technical assistance with EPMA and Sm–Nd isotope analysis. We
214 appreciate the careful editing and constructive comments from Prof. Frank Hawthorne and
215 one anonymous reviewer.

FUNDING

216

217 This research was jointly funded by the National Natural Science Foundation of China
218 (grants 42130102, 42072054 and 41902072).

219 **REFERENCES CITED**

220 Brese, N.E., and O’Keeffe, M. (1991) Bond–valence parameters for solids. *Acta*
221 *Crystallographica*, B47, 192–197.

222 Chen, M.H., Ke, C.H., Tian, Y.F., Chen, G., Ma, K.Z., Ma, S.X., Peng, Y.X., and Zhang, W.
223 (2021) Sedimentary–exhalative massive sulfide deposits in shallow marine environment: a
224 case study from Yushui copper deposit, Guangdong Province. *Acta Geologica Sinica*, 95,
225 1774–1791 (in Chinese with English abstract).

226 Fischer, R.P. (1973) Vanadium, in Brobst, D.A., and Pratt, W.P., eds., *United States Mineral*
227 *Resources: U.S. Geological Survey Professional Paper*, 820, 679–688.

228 Hatch, G.P., (2012) Dynamics in the global market for rare earths. *Elements*, 8, 341–346.

229 Huang, J.H., Huang, F., Evans, L., and Glasauer, S. (2015a) Vanadium: Global (bio)
230 geochemistry. *Chemical Geology*, 417, 68–89.

231 Huang, Y., Sun, X.M., Shi, G.Y., Sa, R.N., Guang, Y., Jiang, X.D., and Que, H.H. (2015b)
232 Re–Os dating of sulphides from the Yushui Cu–polymetallic deposit in eastern
233 Guangdong Province, South China. *Ore Geology Reviews*, 70, 281–289.

234 Liu, P., Gleeson, S.A., Cook, N.J., Lehmann, B., Song, W.L., Bao, Z.A., Jiang, C.Y., Mao,
235 and J.W., 2022, A new potential source of heavy rare earth mineralization: an example
236 from the sediment–hosted Cu deposit of Yushui, South China: submitted to *Geology*.

237 Liu, Z.C., Wu, F.Y., Yang, Y.H., Yang, J.H., Wilde, S.A. (2012) Neodymium isotopic
238 compositions of the standard monazites used in U–Th–Pb geochronology. *Chemical*

- 239 Geology, 334, 221–239.
- 240 Longo, J.M., and Kierkegaard, P. (1970) A refinement of the structure of VO₂. Acta Chemica
241 Scandinavica, 24, 420–426.
- 242 Marezio, M., McWhan, D.B., Remeika, J.P., and Ernier, P.D. (1972) Structural aspects of the
243 metal–insulator transition in Cr–doped VO₂. Physical Review B: Solid State, 5, 2541–
244 2551.
- 245 Momma, K., and Izumi, F. (2011) VESTA 3 for three–dimensional visualization of crystal,
246 volumetric and morphology data. Journal of Applied Crystallography, 44, 1272–1276.
- 247 Sheldrick, G.M. (2015a) SHELXT–Integrated space–group and crystal structure
248 determination. Acta Crystallographica, A71, 3–8.
- 249 Sheldrick, G.M. (2015b) Crystal structure refinement with SHELX. Acta Crystallographica,
250 C71, 3–8.
- 251 Tolosa, A., Alcón, N., Sanmiguel, F., and Ruiz, O. (2011) Method of determining the optical
252 properties of ceramics and ceramic pigments: measurement of the refractive index,
253 Qualicer'12, Castellón, Spain, 1–12.

254 Figure captions

- 255 **Fig. 1.** A. Geological map of the Yushui deposit (After [Huang et al., 2015b](#)). B. Geological
256 cross section of the exploration line a–b in the Yushui deposit ([Chen et al., 2021](#)).
- 257 **Fig. 2.** Photomicrographs showing the occurrence and mineral association of jingwenite–(Y)
258 (Jw–Y). A. euhedral jingwenite–(Y) crystals with bornite (Bn) and chalcopyrite (Ccp). B.
259 anhedral jingwenite–(Y), roscoelite (Rcl), V–HREE–Sc–bearing mineral phase (HREE–V–

260 Sc), quartz and colloidal thortveitite (Tvt) in a matrix of bornite (Bn), chalcopyrite (Ccp), and
261 nolanite (Nol), in reflected light, parallel nicols.

262 **Fig. 3.** Crystal structure of jingwenite-(Y) (unit cell outlined in black lines), plotted with
263 VESTA ([Momma and Izumi, 2011](#)). A. Crystal structure viewed along the *b*-axis, showing the
264 chains of Al-O octahedra (Al1, Al2) and V-O octahedra (V1) linked through isolated Si-O
265 tetrahedra (Si1), forming open cavities occupied by REE (Y1), with hydrogen attached with
266 O7, O8. B. Edge-sharing chains of Al-O octahedra and V-O octahedra parallel to the *b*-
267 axis viewed along the *c*-axis.

268 **Fig. 4.** A. Sm-Nd isochron plot of jingwenite-(Y). B. $\epsilon_{Nd}(t)$ vs. *t* plot of jingwenite-(Y). Data of
269 hingganite-(Y), xenotime and red sandstone are from Liu et al. ([2022](#)).

270

Table captions

271 **Table 1.** Fractional atomic coordinates and displacement parameters (\AA^2) of atoms in
272 jingwenite-(Y).

273 **Table 2.** Selected bond lengths (\AA) and angles ($^\circ$) for jingwenite-(Y).

274 **Table 3.** Calculated bond-valence (*v.u.*) sums for atoms in jingwenite-(Y).

Table 1 (revision 1)

Sites	Wyck.	<i>x</i>	<i>y</i>	<i>z</i>	Occupancy	U_{eq}
Y1	<i>8f</i>	0.25637(3)	0.13540(5)	0.65492(2)	Y _{0.76} Yb _{0.13} Dy _{0.06} Er _{0.05}	0.0118(1)
Al1	<i>4e</i>	0.25	0.87474(25)	0.5	Al _{0.916(15)} V _{0.084(15)}	0.0136(6)
Al2	<i>4e</i>	0.25	0.38344(22)	0.5	Al _{0.66} V _{0.28} Fe _{0.06}	0.0149(3)
V1	<i>8f</i>	0.53026(8)	0.34497(11)	0.74258(4)	V _{0.95} Ti _{0.05}	0.0134(2)
Si1	<i>8f</i>	0.46320(11)	0.62923(17)	0.60704(6)	Si _{1.00}	0.0118(2)
O1	<i>8f</i>	0.42846(31)	0.85038(42)	0.65639(14)	O _{1.00}	0.0132(6)
O2	<i>8f</i>	0.62861(30)	0.63001(43)	0.58226(15)	O _{1.00}	0.0150(6)
O3	<i>8f</i>	0.43379(29)	0.40254(47)	0.65354(14)	O _{1.00}	0.0136(5)
O4	<i>4f</i>	0.35800(30)	0.62789(42)	0.54030(15)	O _{1.00}	0.0141(6)
O5	<i>8f</i>	0.62633(30)	0.63971(42)	0.73683(15)	O _{1.00}	0.0133(6)
O6	<i>8f</i>	0.63489(33)	0.13009(45)	0.72027(16)	O _{1.00}	0.0166(6)
O7(OH)	<i>8f</i>	0.14883(31)	0.13014(44)	0.45881(15)	O _{1.00}	0.0141(6)
O8(OH)	<i>8f</i>	0.36204(31)	0.88768(49)	0.42323(15)	O _{1.00}	0.0152(6)
	U^{11}	U^{22}	U^{33}	U^{23}	U^{13}	U^{12}
Y1	0.0127(2)	0.0138(2)	0.0089(2)	0.0006(0)	0.0010(1)	-0.00004(1)
Al1	0.0164(9)	0.0151(9)	0.0093(8)	0	0.0001(6)	0
Al2	0.0174(7)	0.0163(7)	0.0110(6)	0	0.0011(5)	0
V1	0.0155(3)	0.0147(3)	0.0102(3)	0.0008(2)	0.0003(3)	-0.0021(2)
Si1	0.0124(5)	0.0135(5)	0.0094(5)	-0.0005(3)	0.0004(4)	0.0003(3)
O1	0.0187(14)	0.0137(15)	0.0072(13)	0.0004(9)	0.0013(11)	0.0018(10)
O2	0.0145(14)	0.0190(15)	0.0115(13)	-0.0001(10)	0.0016(11)	-0.0007(10)
O3	0.0141(13)	0.0145(13)	0.0123(13)	0.0008(10)	-0.0026(11)	-0.0006(10)
O4	0.0164(14)	0.0137(14)	0.0122(13)	-0.0005(9)	-0.0011(12)	0.0007(10)
O5	0.0132(13)	0.0147(14)	0.0119(14)	0.0010(9)	0.0007(11)	0.0003(10)
O6	0.0161(13)	0.0199(16)	0.0137(14)	-0.0037(9)	0.0014(12)	0.0020(10)
O7(OH)	0.0137(14)	0.0170(15)	0.0116(13)	0.0007(9)	0.0016(12)	0.0011(10)
O8(OH)	0.0177(14)	0.0166(14)	0.0114(13)	0.0005(10)	0.0031(11)	0.0022(11)

Table 2 (revision 1)

Bond	Length	Bond	Length	Bond	Length
Al1—O8 ^{x2} (OH)	1.833(3)	Al2—O4 ^{x2}	1.929(3)	Si1—O4	1.632(3)
—O4 ^{x2}	1.939(3)	—O7 ^{x2} (OH)	1.942(3)	—O3	1.634(3)
—O7 ^{x2} (OH)	1.951(3)	—O2 ^{x2}	1.972(3)	—O2	1.642(3)
average	1.908	average	1.948	—O1	1.648(3)
				average	1.639
V1—O6	1.664(3)	Y1—O3	2.302(3)	Si1—O4—Al1	3.234(1)
—O5	1.955(3)	—O2	2.312(3)	—O2—Al2	3.427(1)
—O5	1.961(3)	—O6	2.319(3)	—O1—V1	3.181(1)
—O3	1.982(3)	—O1	2.339(3)	—O3—V1	3.178(1)
—O1	1.998(3)	—O5	2.374(3)	Al1—Al2(O7O7)	2.990(2)
—O6	2.406(3)	—O8(OH)	2.381(3)	Al1—Al2(O4O4)	2.888(2)
		—O7(OH)	2.385(3)	V1—V1(O5O6)	3.009(4)
		—O5	2.409(3)		
average	1.994	average	2.353		
Bond	Angle	Bond	Angle	Bond	Angle
Si1—O4—Al1	129.6(2)	Si1—O2—Al2	142.2(1.8)	Si1—O1—V1	151.7(2)
Si1—O3—V1	122.8(2)	Al1—O7—Al2	100.3(1)	Al1—O4—Al2	96.6(1)
V1—O5—V1	100.4(1)	V1—O6—V1	93.5(1)		

Table 3 (revision 1)

	Y1	Al1	Al2	V1	Si1	Sum
O1	0.391 ^{x1↓1→}			0.562 ^{x1↓1→}	0.957 ^{x1↓1→}	1.910
O2	0.427 ^{x1↓1→}		0.442 ^{x2↓1→}		0.979 ^{x1↓1→}	1.848
O3	0.433 ^{x1↓1→}			0.586 ^{x1↓1→}	0.995 ^{x1↓1→}	2.014
O4		0.453 ^{x2↓1→}	0.502 ^{x2↓1→}		0.995 ^{x1↓1→}	1.950
O5	0.341 ^{x2↓2→}			0.626 ^{x2↓2→}		1.934
O6	0.414 ^{x1↓1→}			0.786 ^{x2↓2→}		1.986
O7(OH)	0.344 ^{x1↓1}	0.438 ^{x2↓1→}	0.482 ^{x2↓1→}			1.264
O8(OH)	0.353 ^{x1↓1}	0.595 ^{x2↓1→}				0.948
Sum.	3.044	2.972	2.852	3.972	3.926	

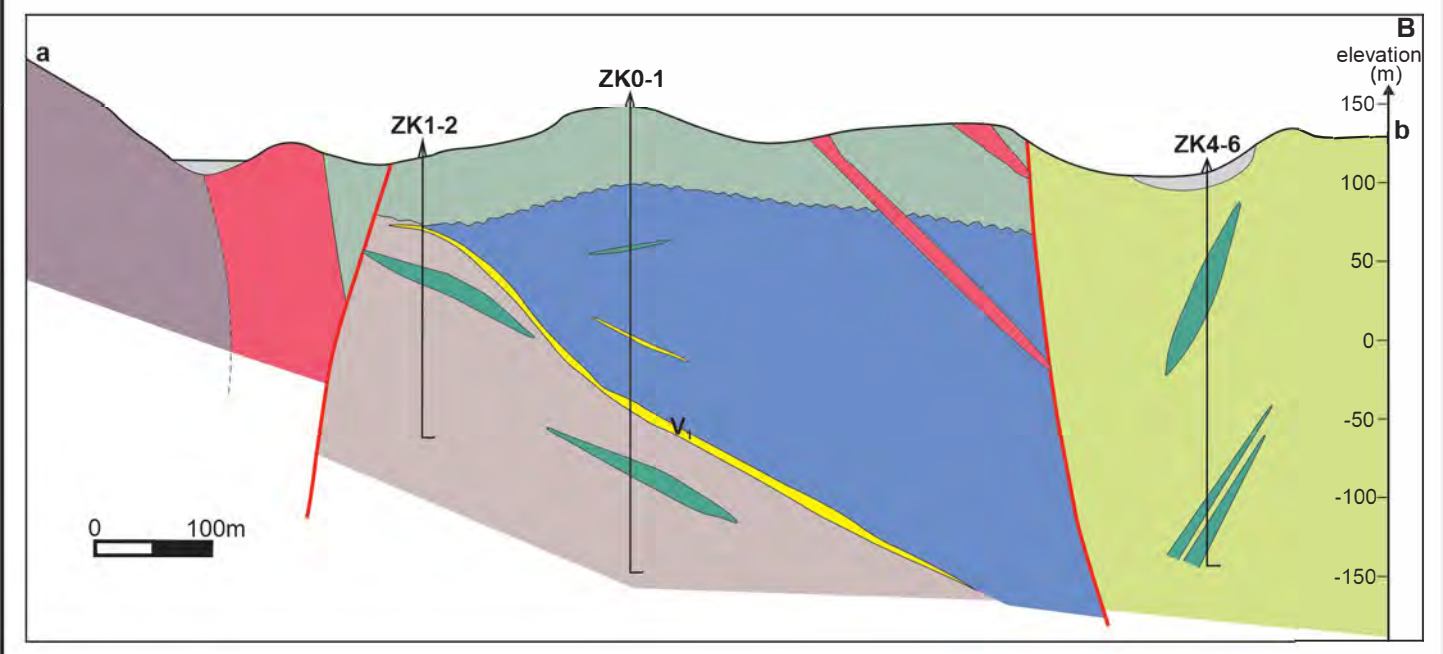
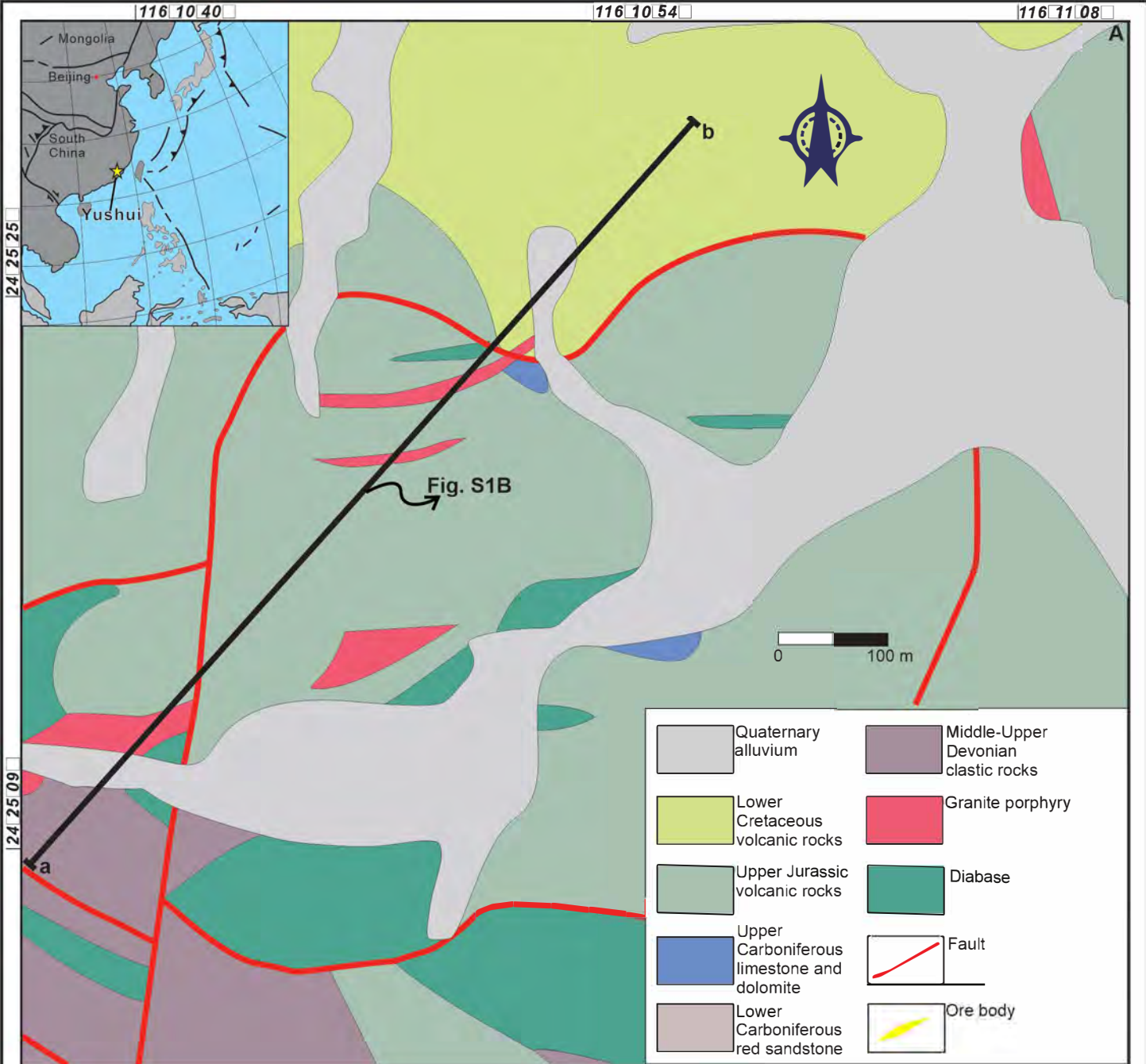


Fig. 1 (revision 1)

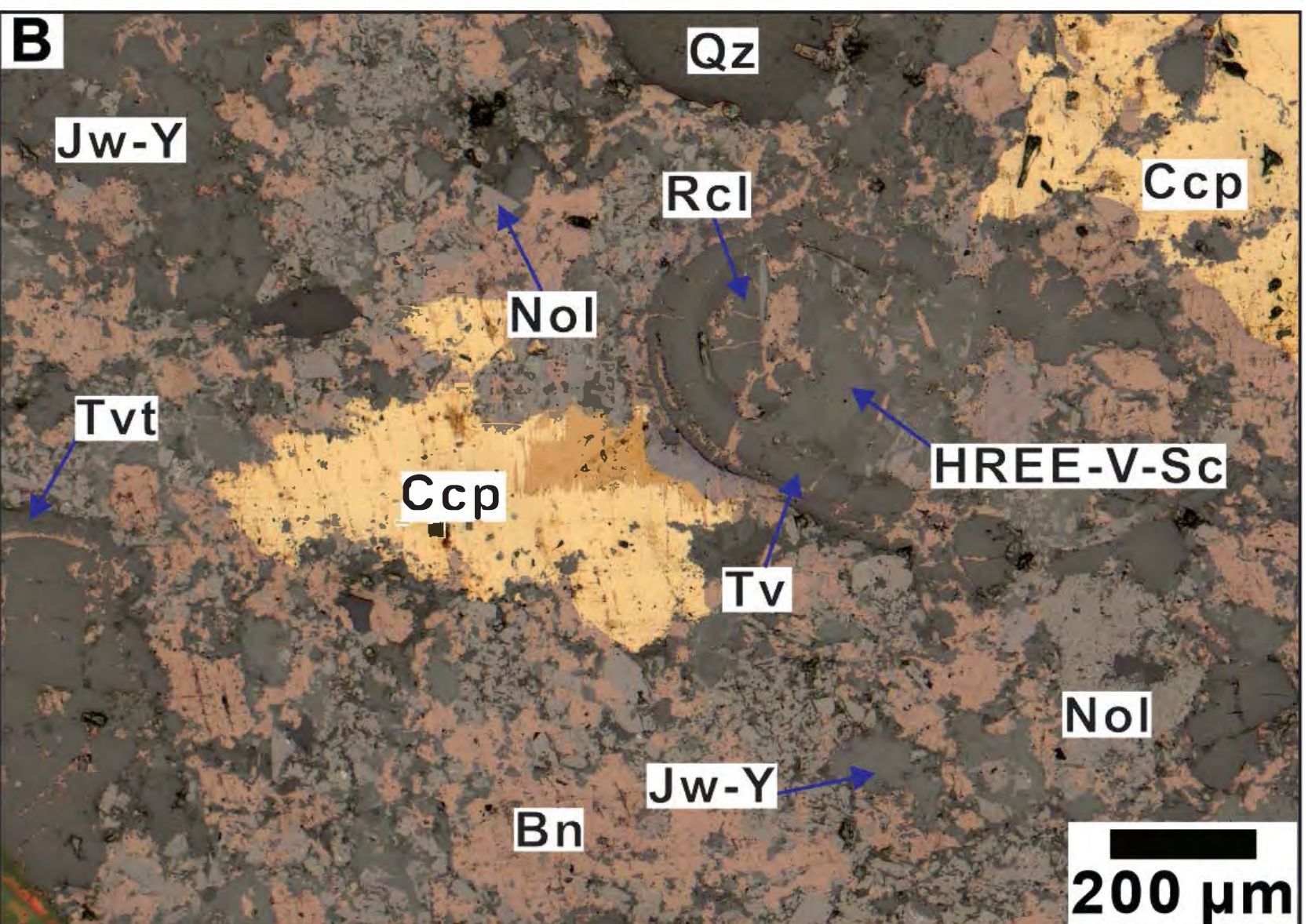
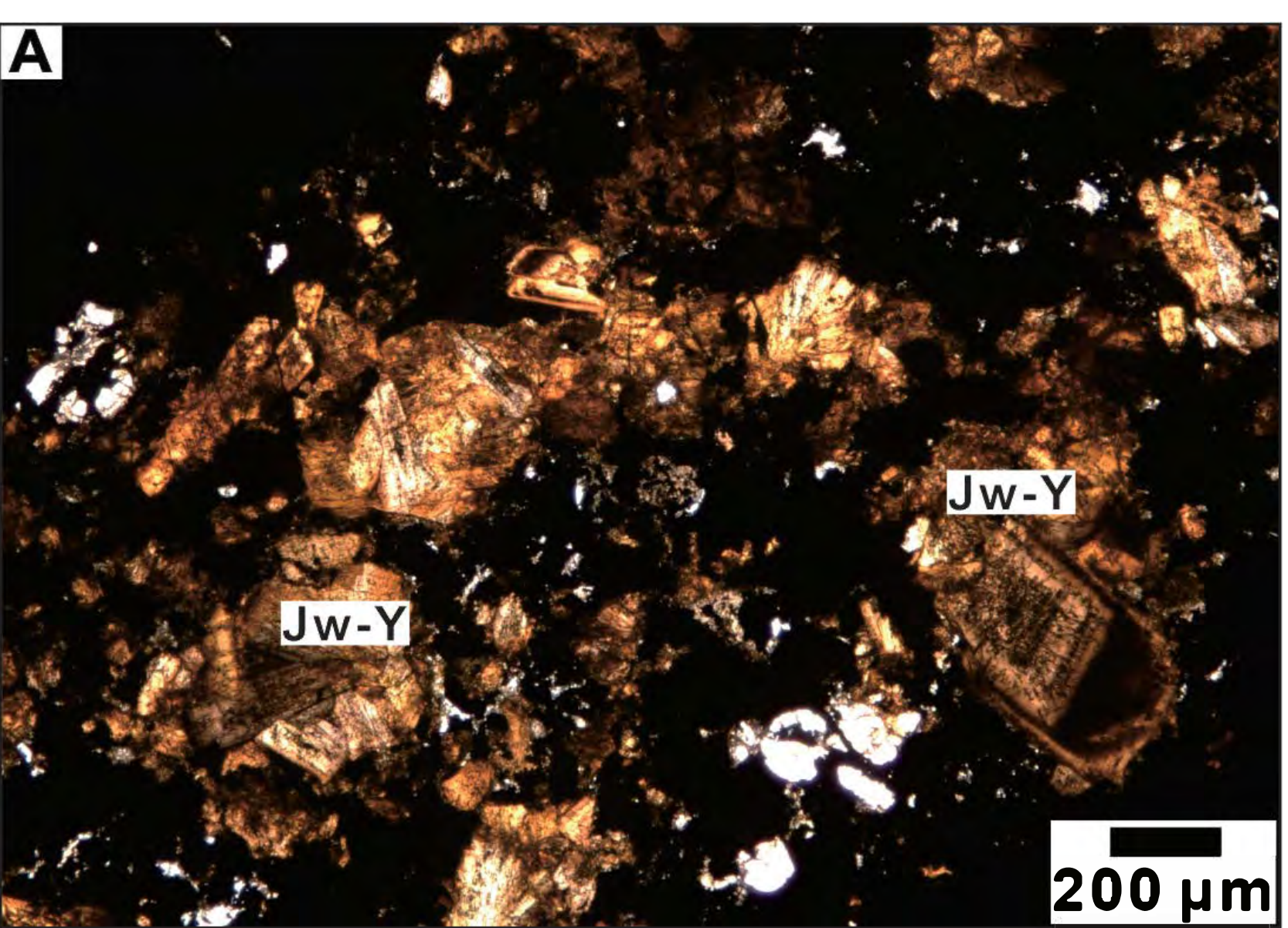
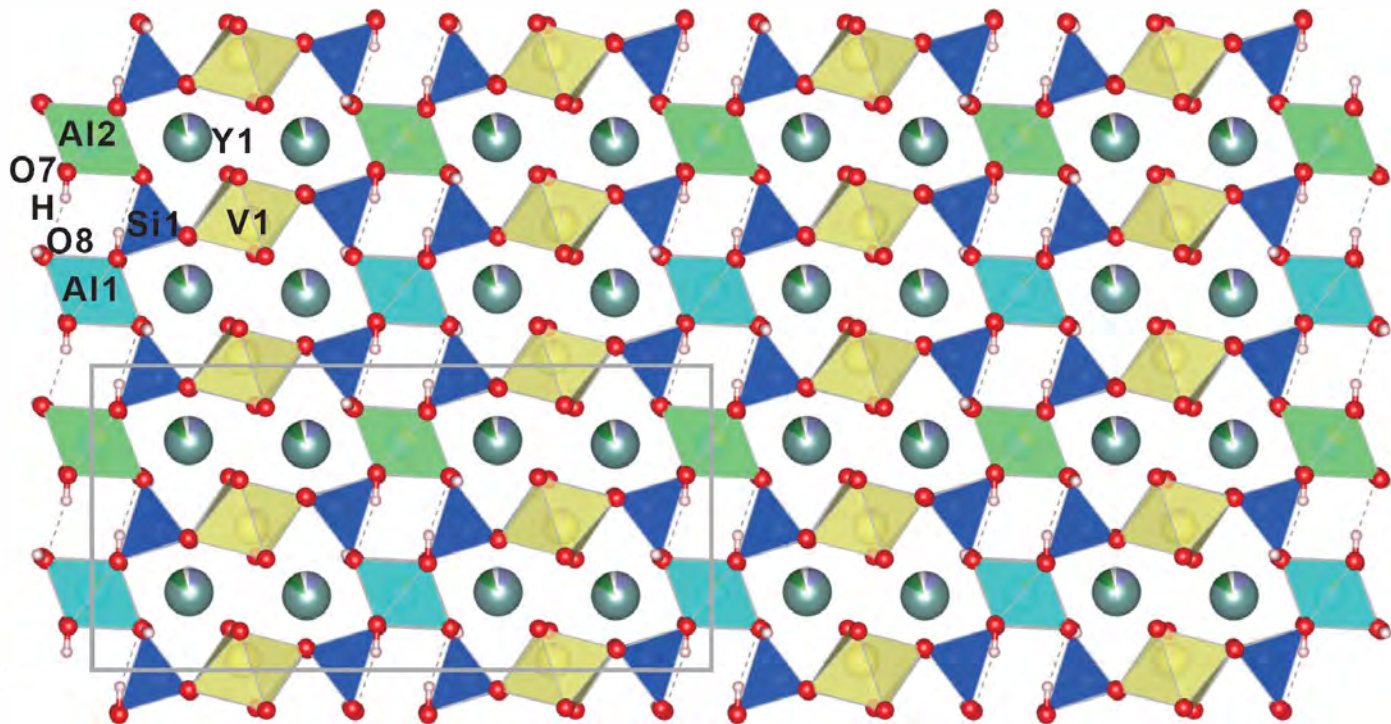


Fig. 2 (revision 1)

A



B

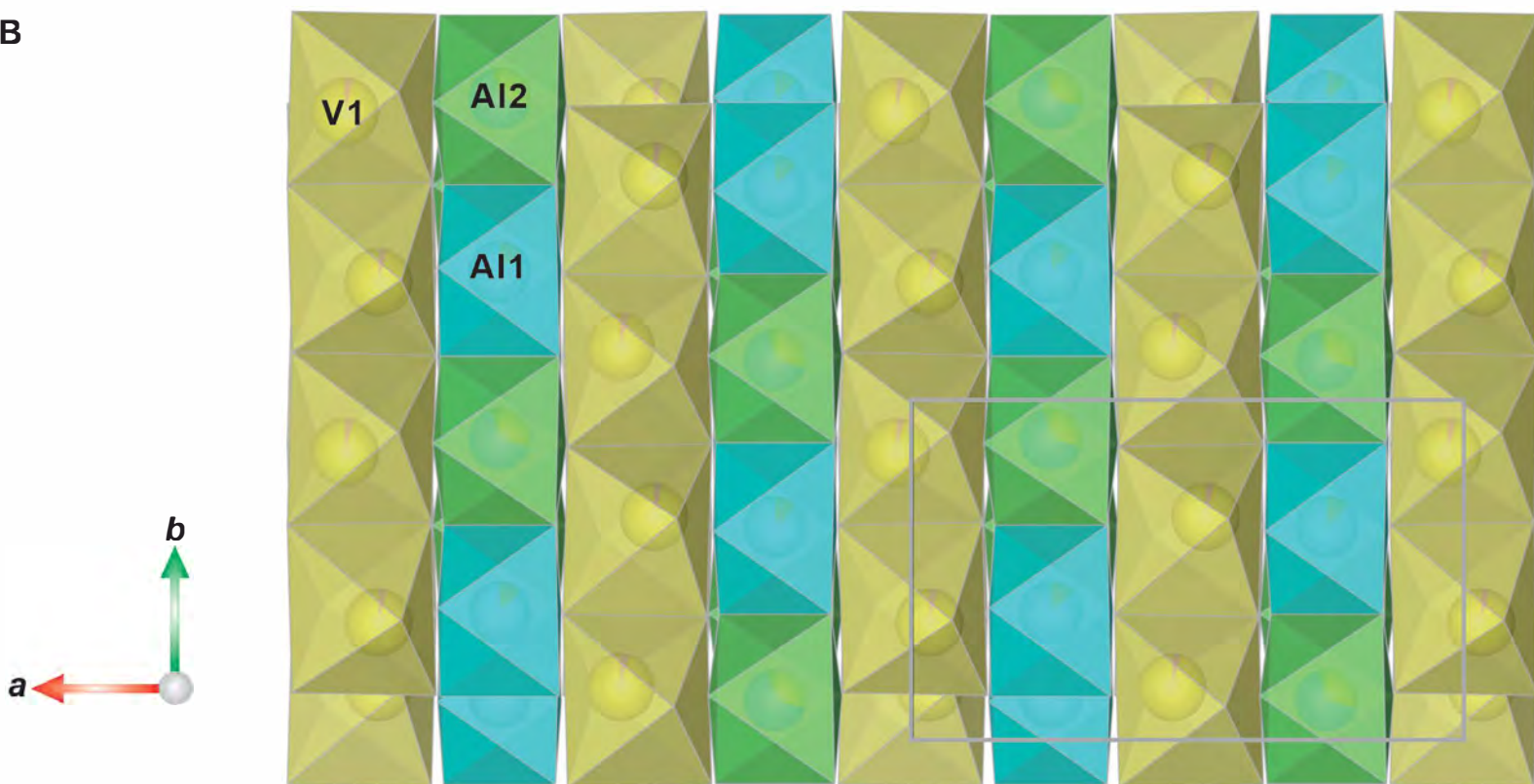


Fig. 3 (revision 1)

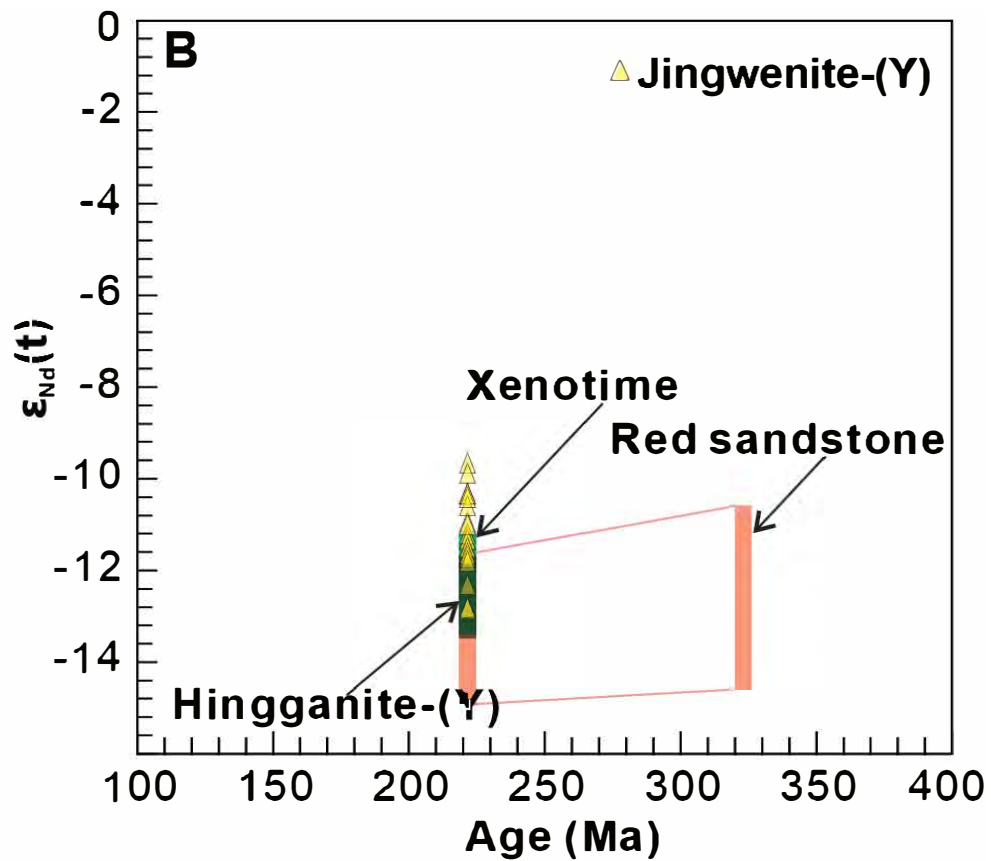
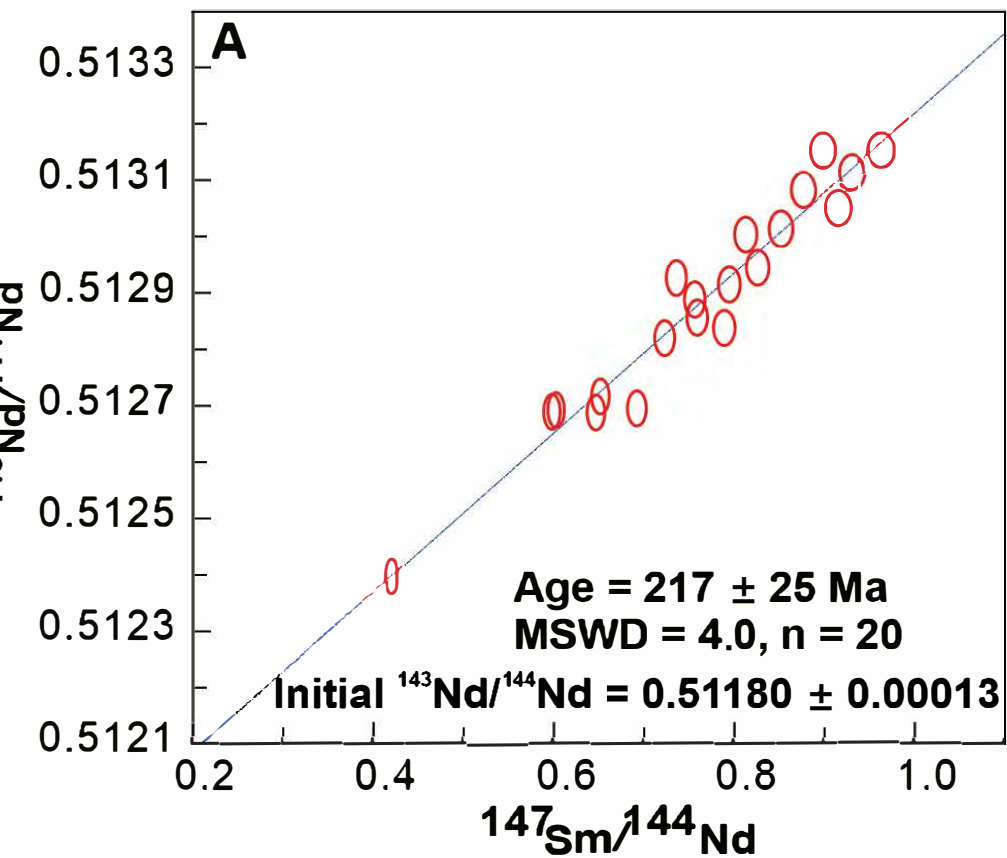


Fig. 4 (revision 1)